Cerebral Cortex, May 2022;32: 1024–1039

https://doi.org/10.1093/cercor/bhab263
Advance Access Publication Date: 10 August 2021
Original Article

ORIGINAL ARTICLE

Progressive Stabilization of Brain Network Dynamics during Childhood and Adolescence

Tianyuan Lei[1,2,3], Xuhong Liao[4], Xiaodan Chen[1,2,3], Tengda Zhao[1,2,3], Yuehua Xu[1,2,3], Mingrui Xia[1,2,3], Jiaying Zhang[1,2,3], Yunman Xia[1,2,3], Xiaochen Sun[5], Yongbin Wei[6], Weiwei Men[7,8], Yanpei Wang[1], Mingming Hu[1], Gai Zhao[1], Bin Du[1], Siya Peng[1,2,3], Menglu Chen[1,2,3], Qian Wu[1,3], Shuping Tan[9], Jia-Hong Gao[7,8,10], Shaozheng Qin[1,2,3,11], Sha Tao[1], Qi Dong[1] and Yong He[1,2,3,11]

[1]State Key Laboratory of Cognitive Neuroscience and Learning, Beijing Normal University, Beijing 100875, China, [2]Beijing Key Laboratory of Brain Imaging and Connectomics, Beijing Normal University, Beijing 100875, China, [3]IDG/McGovern Institute for Brain Research, Beijing Normal University, Beijing 100875, China, [4]School of Systems Science, Beijing Normal University, Beijing 100875, China, [5]Department of Linguistics, Beijing Language and Culture University, Beijing 100083, China, [6]Department of Complex Trait Genetics, Center for Neurogenomics and Cognitive Research, VU University Amsterdam, 1081 HV Amsterdam, the Netherlands, [7]Center for MRI Research, Academy for Advanced Interdisciplinary Studies, Peking University, Beijing 100871, China, [8]Beijing City Key Laboratory for Medical Physics and Engineering, Institute of Heavy Ion Physics, School of Physics, Peking University, Beijing 100871, China, [9]Beijing Huilongguan Hospital, Peking University Huilongguan Clinical Medical School, Beijing 100096, China, [10]IDG/McGovern Institute for Brain Research, Peking University, Beijing 100871, China and [11]Chinese Institute for Brain Research, Beijing 102206, China

Address correspondence to Xuhong Liao. E-mail: liaoxuhong@bnu.edu.cn, Yong He. E-mail: yong.he@bnu.edu.cn

Abstract

Functional brain networks require dynamic reconfiguration to support flexible cognitive function. However, the developmental principles shaping brain network dynamics remain poorly understood. Here, we report the longitudinal development of large-scale brain network dynamics during childhood and adolescence, and its connection with gene expression profiles. Using a multilayer network model, we show the temporally varying modular architecture of child brain networks, with higher network switching primarily in the association cortex and lower switching in the primary regions. This topographical profile exhibits progressive maturation, which manifests as reduced modular dynamics, particularly in the transmodal (e.g., default-mode and frontoparietal) and sensorimotor regions. These developmental refinements mediate age-related enhancements of global network segregation and are linked with the expression profiles of genes associated with the enrichment of ion transport and nucleobase-containing compound transport. These results highlight a progressive stabilization of brain dynamics, which expand our understanding of the neural mechanisms that underlie cognitive development.

Key words: brain development, connectomics, gene expression, resting-state fMRI

Introduction

The human brain is an efficient and dynamic information processing system with a complex spatiotemporal organization. Network science approaches have revealed that the human brain functional network contains a nontrivial modular structure, in which functional specialization and integration are well balanced at low wiring cost (He et al. 2009; Meunier et al. 2010; Sporns and Betzel 2016; Liao et al. 2017). This modular structure facilitates a fast response to domain-specific stimuli (Meunier et al. 2010; Bertolero et al. 2015; Sporns and Betzel 2016) and also enables efficient global brain communication (Bullmore and Sporns 2012). Recent studies suggest that the modular organization of the brain is not static but rather shows temporally varying patterns over short time scales (e.g., seconds), with higher network switching primarily in the association (e.g., frontoparietal) regions and lower variability in the primary regions (Chen et al. 2016; Liao et al. 2017; Pedersen et al. 2018; Liu et al. 2020). These network dynamics contribute significantly to flexible cognitive function (Chen et al. 2016; Liao et al. 2017; Yin et al. 2020) and are distinctive to each individual (Liao et al. 2017). During short-term training, network segregation in the brain is increased through dynamic reconfigurations, and these increases correspond to improved task automation (Bassett et al. 2015; Finc et al. 2020). These findings suggest a link between adaptive network dynamics and skill acquisition which we believe may be significant not only during short-term learning but also in long-term development. However, how network dynamics changes during childhood and adolescence, a crucial stage for cognitive and behavioral development, remains largely unknown. The goal of the current study was to gain insight into the principles shaping the maturation of network dynamics in human brain, and its connection with cognitive development and gene expression profiles.

Childhood and adolescence are critical developmental phases for the consolidation and refinement of individual motor, cognitive, social, and emotional capabilities (Berk 2017). These physical, cognitive, and psychological developments occur in parallel with the substantial development of brain architecture (Vértes and Bullmore 2015; Cao et al. 2016). During this period, brain microstructure is fine-tuned through processes including regressive synaptic pruning and progressive myelination (Tau and Peterson 2010; Vértes and Bullmore 2015). At the macroscopic level, the modular structure of the functional brain networks undergoes remarkable reconfiguration with age (Vértes and Bullmore 2015; Cao et al. 2016; Grayson and Fair 2017), shifting from anatomical proximity during childhood to a spatially distributed layout at adulthood (Fair et al. 2009). Within modules, a decrease in the number of short-range connections with age is observed in some modules as a result of synaptic pruning (Fair et al. 2007; Supekar et al. 2009), while in others, the number of long-range connections increases over time, for example the increase in anterior–posterior connections observed in the default-mode network (Fair et al. 2008; Sato et al. 2014; Fan et al. 2021). Between modules, integration between the default-mode network and other brain systems exhibits an age-related increase, while integration between the higher order cognitive network and the subcortical network with other brain systems show an age-related decrease (Gu et al. 2015). These system-specific changes in intramodule and intermodule connections are indicative of the growing functional differentiation of brain modules with development. Notably however, previous studies on brain network modularity were mainly undertaken on the development of static (i.e., time-invariant) modular architecture, and largely ignored the temporal dynamics of brain modularity. Yet, as recent work has pointed out, cognitive growth is largely dependent on age-related adjustments in the brain's temporal dynamics (Hutchison and Morton 2016). To date, how modular dynamics in the brain network develops toward maturation over childhood to adolescence has yet to be established.

Structural and functional development of the brain is shaped by genetic factors (Johnson et al. 2009; Douet et al. 2014; Zhong et al. 2018). For instance, animal model studies have revealed that myelination in the central neural system is closely governed by a gene named the myelin gene regulatory factor, which is specifically expressed in oligodendrocytes (Emery et al. 2009), and synaptic pruning is mediated by astrocytes through the *Megf10* (i.e., multiple epidermal growth factor-like domains protein 10) and *Mertk* (i.e., Mer tyrosine kinase) phagocytic pathways (Chung et al. 2013). Recent advances in connectome-transcriptome association analysis now enable us to explore the transcriptional signatures underlying the spatial organization of the human brain network *in vivo* (Fornito et al. 2019). In adults, the spatial layout of functional modules is shaped by genes associated with the enrichment of ion channels (Richiardi et al. 2015). Intermodule hubs have also been shown to be metabolically expensive, with an overrepresentation of genes for oxidative metabolism and mitochondria (Vértes et al. 2016). A very recent study reported that the spatial layout of brain module dynamics in adults is associated with genes involved in potassium ion transport, establishing a link between large-scale connectivity dynamics and transcriptional profiles (Liu et al. 2020). Nevertheless, little is known on how gene expression is linked to developmental brain dynamics in children.

To address these issues, we investigated the developmental changes in brain network dynamics between childhood and adolescence, and the transcriptional profiles of genes related to this process. Brain network analyses were undertaken using a large longitudinal resting-state functional magnetic resonance imaging (rsfMRI) dataset comprising scans from 305 healthy children (age 6–14 years, 491 scans in total) (Fan et al. 2021), and genetic analysis was conducted using postmortem gene expression data from the Allen Human Brain Atlas (Hawrylycz et al. 2012). Specifically, for all rsfMRI scans of each participant, we applied a multilayer network model (Mucha et al. 2010) to identify the time-resolved modular architecture in the child brain and further quantified the temporal switching of regional module affiliations. We aimed to investigate i) developmental patterns in brain network dynamics during childhood and adolescence at the whole-brain, system and nodal levels, and their potential association with cognitive development; ii) whether these developmental patterns contribute to age-related changes in the information transmission capability of brain networks; and iii) the association between developmental changes in brain network dynamics and gene transcriptional profiles.

Materials and Methods

Participants

We utilized a longitudinal rsfMRI dataset consisting of scans obtained from 360 typically developing children (F/M = 163/197, 6 to 14 years, 643 scans in total) collected by the Children School Functions and Brain Development Project (Beijing Cohort). Participants included in this study were cognitively normal, and had no history of neuropsychiatric illness, psychoactive drug use,

significant head injuries, or significant physical illness. Some of these children underwent multiple sessions of multimodal MRI imaging (T1, T2, rsfMRI etc.) with an interval of approximately 1 year between each session. After strict quality control screening (see Supplement for further details), 491 rsfMRI scans of 305 children (F/M = 143/162, 6 to 14 years) were retained for use in our study (Fig. 1A). These were made up of three scans from 47 children (F/M = 31/16), two scans from 92 children (F/M = 47/45), and a single scan from 166 children (F/M = 65/101). For the purposes of comparison, we also used an rsfMRI dataset comprising data from 61 healthy young adults (F/M = 37/24, 18 to 29 years), which was acquired using an identical scanner and scanning protocols. The study was approved by the Ethics Committee of Beijing Normal University, and written informed consent was obtained from all participants or their parents/guardians.

Imaging Data Acquisition

MRI data were acquired using a 3 T SIEMENS Prisma scanner in the Center for Magnetic Resonance Imaging Research at Peking University. Both children and adults were scanned using the same scanner and identical scanning protocols. For each participant (child and adult), structural and functional MRI scans were acquired using the following protocols. T1-weighted images were acquired using a sagittal 3D magnetization prepared rapid acquisition gradient echo (MPRAGE) sequence: repetition time (TR) = 2530 ms, echo time (TE) = 2.98 ms, inversion time = 1100 ms, flip angle (FA) = 7°, matrix = 256 × 224, field of view (FOV) = 256 × 224 mm^2, slice number = 192, slice thickness = 1 mm, bandwidth = 240 Hz/Px. The rsfMRI data were acquired using an echo-planar imaging sequence: TR = 2000 ms, TE = 30 ms, FA = 90°, matrix = 64 × 64, FOV = 224 × 224 mm^2, slice number = 33, slice thickness/gap = 3.5/0.7 mm, scan duration = 8 min (i.e., 240 volumes in total). The participants were asked to keep a fixation on a bright cross-hair in the center of the scanner screen. A field map was acquired prior to the rsfMRI scan using a 2D dual gradient-echo sequence: TR = 400 ms, TE1 = 4.92 ms, TE2 = 7.38 ms, FA = 60°, matrix = 64 × 64, FOV = 224 × 224 mm^2, slice number = 33, slice thickness/gap = 3.5/0.7 mm.

Imaging Data Preprocessing

Resting state fMRI data from the child cohort were preprocessed using SPM12 (https://www.fil.ion.ucl.ac.uk/spm) and DPABI 3.0 (Yan et al. 2016). First, for each scan, we removed the first 10 volumes and performed slice-timing correction. Next, a field map correction was applied to remove geometric distortion. We then performed head motion correction and estimated the mean framewise displacement (FD) (Power et al. 2012) across time for each scan. A total of 94 scans were excluded due to excessive head motion (i.e., translation > 3 mm, rotation > 3°, or mean FD > 0.5 mm). The functional images were then coregistered with individual T1 images and spatially normalized to a custom template using a unified segmentation algorithm (Ashburner and Friston 2005) (see Supplement for further details). During initial segmentation of the T1 images, Chinese Pediatric Atlases (CHN-PD) (6–12 years) (Zhao et al. 2019) were used as the reference for segmentation to improve accuracy in the spatial deformation of pediatric brain images. The normalized functional images were resampled to 3-mm isotropic voxels and spatially smoothed with a Gaussian smoothing kernel (full-width at half maximum = 4 mm). Next, we performed linear detrending, nuisance signal regression, and temporal band-pass filtering (0.01–0.1 Hz). During nuisance regression, the following nuisance regressors were included to reduce the influence of nonneural signals: Friston's 24 head motion parameters (Friston et al. 1996), "bad" time points with FD above 0.5 mm, and white matter, cerebrospinal fluid and global brain signals.

Functional images from the adult cohort were preprocessed using the same procedures, except that when undertaking spatial normalization, functional images from the adult group were spatially normalized to the Montreal Neurological Institute (MNI) standard space.

Construction of Dynamic Functional Networks

The selection of an appropriate brain parcellation scheme is essential for node definition in the construction of functional networks (Bullmore and Bassett 2011). For functional networks constructed from the child scans, we defined network nodes based on a customized random parcellation scheme, referred to as random-1024 parcellation, comprising 1024 gray matter regions of uniform sizes (Zalesky et al. 2010). The time course for each node was extracted by averaging the time courses across voxels within the node. We then applied a commonly used sliding window approach (window length = 60 s, step size = 1 TR (i.e., 2 s), total windows for each scan = 201) to estimate dynamic functional connectivity over time (Hutchison et al. 2013; Lurie et al. 2020). Specifically, internode functional correlations were estimated within each window using the Pearson's correlation coefficient between nodal time courses. The resulting networks were then thresholded by applying a network density of 5% to remove weak or spurious connections, producing a time-varying binary functional network for each rsfMRI scan of each child. Negative correlations were eliminated prior to network thresholding due to their ambiguous physiological interpretation (Fox et al. 2009; Murphy and Fox 2017).

Functional networks from the adult scans were constructed using the same procedures. To enable regional-level comparisons between the child and adult networks, we obtained the parcellation scheme for the adult networks by spatially transforming the random-1024 parcellation from the children's custom space to the MNI space.

Identification of Dynamic Modular Architecture

We employed a multilayer network model (Mucha et al. 2010), which can incorporate connectivity information within adjacent time windows, to identify the dynamic modular structure in the child and adult brain networks. Specifically, the dynamic functional networks in each scan were considered as a multilayer network consisting of 201 time-ordered layers (i.e., windows) with ordinal interlayer coupling, in which identical nodes in adjacent layers were coupled with nonzero strength (Fig. 1B). Then, we identified the time-resolved modular architecture by optimizing the modularity, Q_{mod}, of the multilayer network, with an implicit assumption that module change between layers was continuous. The modularity, Q_{mod}, of the time-varying modular structure is defined as (Mucha et al. 2010):

$$Q_{mod}(\gamma,\omega) = \frac{1}{2\mu}\sum_{ijlr}\left[\left(A_{ijl}-\gamma_l\frac{k_{il}k_{jl}}{2m_l}\right)\delta(l,r)+\delta(i,j)\,\omega_{jlr}\right] \times \delta\left(M_{il},M_{jr}\right), \quad (1)$$

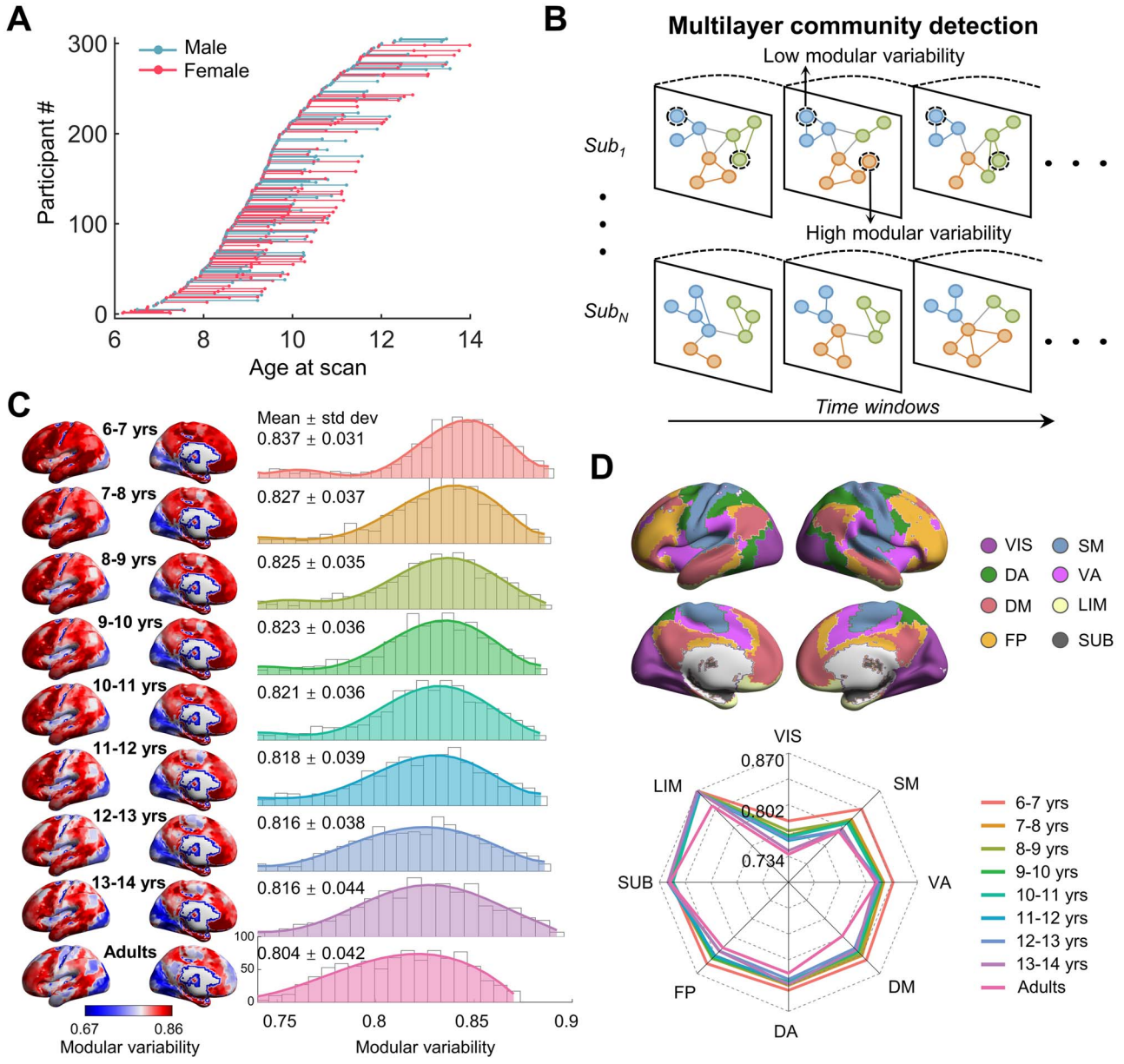

Figure 1. Age distribution of child participants and multilayer module dynamics at different ages. **(A)** Age information of child participant scans. **(B)** Schematic diagram of the multilayer network model and regional modular variability. Each layer represents a functional network within a sliding window. In addition to connections within the same layer, each node also connects to itself in adjacent layers. **(C)** Spatial patterns and frequency polygons of modular variability across the 1024 nodes for each child subgroup and for the adult group. **(D)** Top: spatial location of eight functional systems (i.e., seven cortical systems (Yeo et al. 2011) and one subcortical system (Tzourio-Mazoyer et al. 2002). Bottom: distribution of the mean modular variability value of each functional system for each child subgroup and for the adult group. Cortical data were mapped using the BrainNet Viewer software (Xia et al. 2013). VIS, visual; SM, somatomotor; DA, dorsal attention; VA, ventral attention; DM, default-mode; LIM, limbic; FP, frontoparietal; SUB, subcortical.

where variables i and j are node labels, and variables l and r are layer labels. Specifically, μ represents the total connectivity strength of the entire network, m_l denotes the total connectivity strength within layer l, A_{ijl} denotes the connectivity strength between node i and node j in layer l, $k_{il}k_{jl}/2m_l$ denotes the connection probability expected by chance between node i and node j in layer l, k_{il} denotes the degree of node i in layer l, and M_{il} denotes the module label of node i in layer l. The function δ (x, y) is equal to 1 if variable x is identical to variable y, and is equal to 0 in all other cases. Parameters γ and ω are, respectively, the topological resolution parameter and temporal coupling parameter. Parameter γ determines the module size. The larger the value of γ, the smaller the size of the identified modules, and the greater the number of modules in the network. Here, we used the commonly used default value of $\gamma = 1$ (Bassett et al. 2011; Braun et al. 2015). Parameter ω determines the extent of interlayer interaction. The smaller the value of ω, the more independent the adjacent layers. We chose $\omega = 1$ to balance the influence of interlayer and intralayer edges (when $\omega < 1$, intralayer edge strength dominates modularity optimization)

(Bassett et al. 2011; Braun et al. 2015). Notably, the dynamic modular architecture varies slightly with each instance of identification since the heuristic Louvain algorithm (Blondel et al. 2008) is applied in the modularity optimization. Here, all measurements relating to dynamic modular architecture were taken as the average across 100 instances of identification. The module detection algorithm for multilayer networks was obtained from an open MATLAB code package at http://netwiki.amath.unc.edu/GenLouvain/GenLouvain (Mucha et al. 2010).

Modular Variability Analysis

To characterize the temporal reconfiguration of functional modular architecture, we tracked the change in functional modules across windows. Specifically, we assessed the change in module affiliation (i.e., network switching) over time for all nodes using a measure of modular variability (Liao et al. 2017). First, given a node i, we evaluated the variability of its module affiliation between any two windows t and t' (Steen et al. 2011) as

$$ModVar_i(t,t') = 1 - \frac{|M_i(t) \cap M_i(t')|^2}{|M_i(t)| \cdot |M_i(t')|}, \quad t \neq t', \tag{2}$$

where $M_i(t)$ denotes the module to which node i belonged in window t, $|M_i(t)|$ represents the number of nodes included in module $M_i(t)$, and $|M_i(t) \cap M_i(t')|$ represents the number of nodes in the intersection between modules $M_i(t)$ and $M_i(t')$. A small intersection between two modules indicates large variability. Secondly, we calculated the total modular variability of a node over all time windows (Liao et al. 2017) as

$$ModVar_i = \sum_{t=1}^{N} w(t) \cdot ModVar_i(t), \tag{3}$$

where $ModVar_i(t) = \frac{1}{N-1}\sum_{t' \neq t} ModVar_i(t,t')$ denotes the modular variability of node i between window t and all other windows, and N denotes the total number of windows. A normalized weighted coefficient $w(t)$ is employed in Eq. (3) to reduce the impact of potential outlier windows. The coefficient $w(t)$ is a measure of interwindow similarity in the modular structure, which is calculated using adjusted mutual information (Vinh et al. 2010), and denotes the overall similarity of the modular structure in window t with that in all other windows. For each rsfMRI scan, we calculated the modular variability of each of the 1024 nodes. The larger the nodal modular variability, the more often the node tends to switch between modules over time. The mean modular variability of the whole brain was calculated as the average modular variability across all nodes.

To illustrate the change in modular variability patterns with development, we divided all child rsfMRI scans into eight subgroups, with a 1-year interval between each subgroup. A group-level modular variability map was generated for each subgroup by averaging individual maps within each subgroup. To enable comparison, a group-level modular variability map for the young adults was also generated. We then conducted Pearson's correlation analyses to measure the spatial similarity between modular variability maps of all child subgroups and the adult group. To correct for spatial autocorrelation, we generated 10 000 surrogate maps constrained by the spatial autocorrelation characteristics of the modular variability map of the adult group (Burt et al. 2020), and obtained a null distribution of correlation coefficients for each child subgroup. Empirically observed spatial similarity values were compared against the null distribution to determine significance levels. To further assess the system dependence of nodal modular variability, we categorized the 1024 nodes into eight functional systems. Seven of these systems were obtained from a prior functional system parcellation scheme (Yeo et al. 2011): the visual, somatomotor, dorsal attention, ventral attention, limbic, frontoparietal, and default-mode systems. The remaining subcortical system was extracted from the Automated Anatomical Labeling atlas (Tzourio-Mazoyer et al. 2002). When analyzing system-dependence in children, the functional system atlases defined from adults were spatially transformed to the children's custom space prior to the allocation of nodes to their respective functional systems. Finally, we quantified the age-related changes in regional modular variability using a mixed effect model.

Relationship Between Developmental Changes in Brain Network Dynamics and Cognitive Function

We explored the cognitive significance of regions showing significant developmental changes in modular variability using the NeuroSynth meta-analytic database (www.neurosynth.org) (Yarkoni et al. 2011). Specifically, we examined the cognitive terms associated with the regions exhibiting significant age-related decreases in modular variability, which made up the majority of brain areas showing developmental changes. These regions were predominantly located in six functional systems (hereafter referred as source systems), including somatomotor, default-mode, frontoparietal, dorsal attention, ventral attention, and visual systems (Fig. 2B). We first generated six thresholded t-maps denoting age effects on regions of interest within each source system separately. Next, we quantified the Pearson's correlation between each t-map and all cognitive term maps available from the NeuroSynth database. The results were illustrated using word-cloud plots.

Module Co-occurrence Analysis at the System Level

To explore whether the developmental changes in nodal modular variability were associated with the dynamic interplay between functional systems, we examined the age-related changes in module co-occurrence of different systems. Since most nodes exhibiting significant age effects showed linear decreases with age (Fig. 2B), we focused our analysis on nodes showing a significant negative age effect (N_s nodes in total). Briefly, we calculated the module co-occurrence probability of each node showing significant age effects with each of the other nodes in the brain network as the percentage of time windows in which the two nodes belonged to the same module (Braun et al. 2015). For all scans of each child, an $N_s \times 1024$ co-occurrence matrix was obtained (Fig. 2D). Next, the module co-occurrence matrix was summarized at the system level by calculating the average co-occurrence probability of nodes in each source system with nodes in each of the target systems. (Source systems are those containing nodes showing significant age-related decreases, i.e., the somatomotor, default-mode, frontoparietal, dorsal attention, ventral attention, and visual systems. Target systems refer to all eight functional systems.) Therefore, for all scans of each child, we obtained a

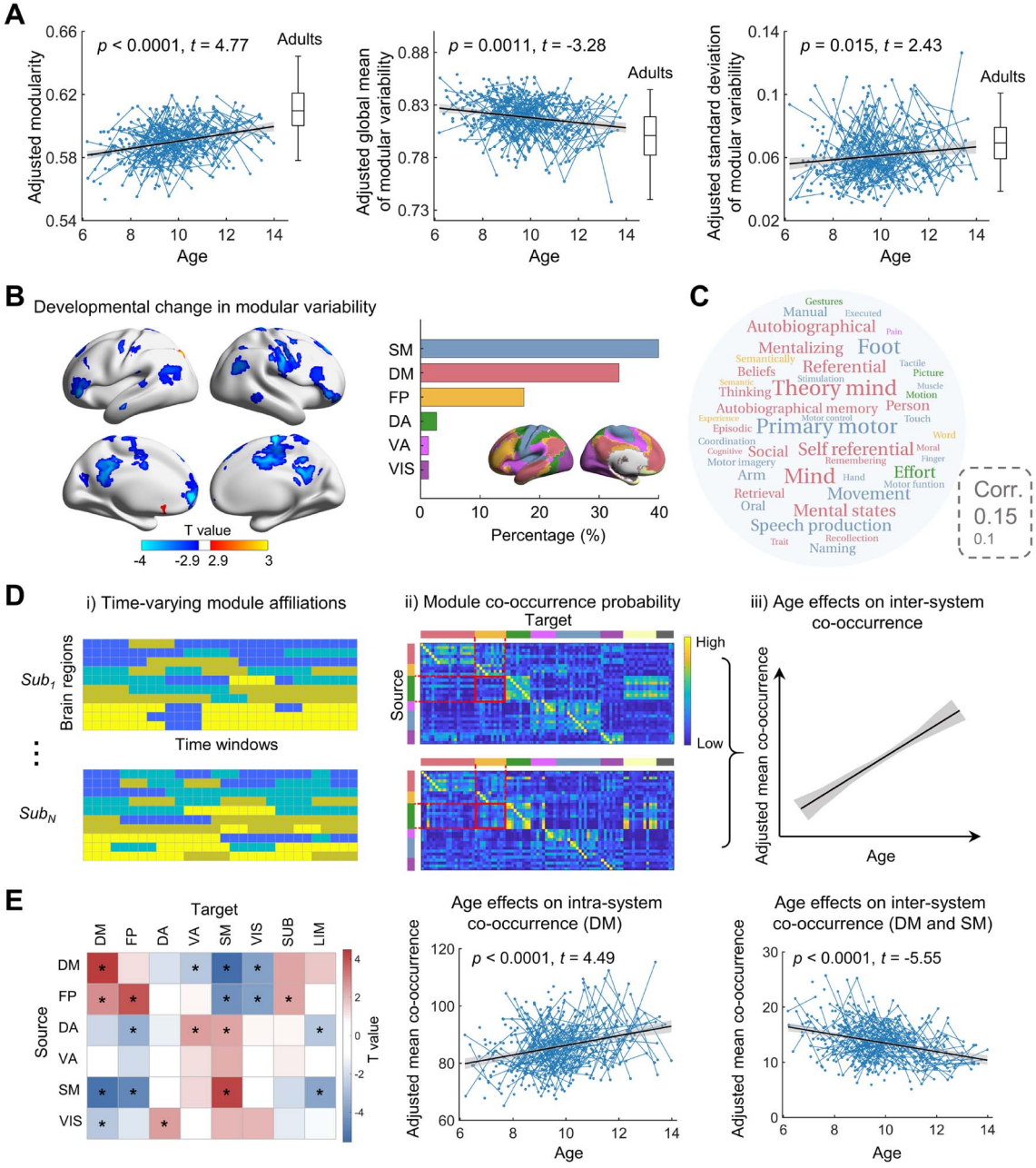

Figure 2. Longitudinal development of brain network dynamics in children. **(A)** Age effects on the network modularity and the mean and standard deviation of the whole brain modular variability. Boxplots represent the distribution median, and the 25th and 75th percentiles of the adult group. **(B)** Left: Spatial distribution of regions showing significant developmental changes in modular variability between childhood and adolescence. Age effects are displayed in terms of *T* values (FDR-corrected $P < 0.05$). Right: proportion of regions with significant age-related decreases found in each functional system. **(C)** Cognitive terms associated with regions showing significant age-related decreases in modular variability, which was obtained based on the NeuroSynth meta-analytic database (Yarkoni et al. 2011). Font sizes of the cognitive terms represent the correlation coefficients between the regions of interest and the cognitive term maps. Font colors correspond to different functional systems. **(D)** Schematic diagram of module co-occurrence at the system level. Left: regional module affiliations at each time window. Middle: matrix showing the modular co-occurrence probability between the six source systems and each of the eight functional systems (target systems). Each element in the matrix represents the percentage of time windows in which two nodes from different systems belonged to the same module. Right: estimated age effects on the mean co-occurrence of every system pair. **(E)** Significant developmental effects on modular co-occurrence probability at the system level. Left: age effects on co-occurrence probability (*, $P < 0.05$, FDR corrected). Middle: age effect on the mean co-occurrence probability for nodes within the default-mode system. Right: age effect on the mean co-occurrence probability of nodes in the default-mode system with those in the somatomotor system. We used a mixed effect model to estimate age effects. In **(A)** and **(E)**, the blue lines connecting scattered points represent longitudinal scans of the same child. The adjusted value denotes the measure of interest corrected for sex, head motion, and random age effects. VIS, visual; SM, somatomotor; DA, dorsal attention; VA, ventral attention; DM, default-mode; LIM, limbic; FP, frontoparietal; SUB, subcortical.

6×8 module co-occurrence matrix at the system level, each row of which denoted the co-occurrence probability of a source system with each of the target systems. Finally, we assessed the age-related changes in the co-occurrence probability for each pair of systems using a mixed effect model. The significance level was corrected for multiple (i.e., 48) comparisons at the system level using the false discovery rate (FDR) method (corrected $P < 0.05$).

Relationship Between Age, Brain Dynamics and Network Efficiency

To explore whether dynamic modular reconfiguration was related to information communication capabilities in the brain network, we considered two global network metrics, global efficiency and local efficiency, to capture different aspects of information transmission efficiency.

Global efficiency (E_{glob}). Global efficiency measures information transmission efficiency across all pairs of nodes in the network (Latora and Marchiori 2001; Rubinov and Sporns 2010). In a given network, E_{glob} is defined as

$$E_{glob} = \frac{1}{N(N-1)} \sum_{i,j=1}^{N} \frac{1}{d_{ij}}, i \neq j, \quad (4)$$

where N represents the total number of nodes in the network, and d_{ij} is the shortest path length between node i and node j. E_{glob} of the dynamic brain network was calculated as the average E_{glob} across all time windows.

Local efficiency (E_{loc}). Local efficiency measures information communication efficiency among local subgraphs (Latora and Marchiori 2001; Rubinov and Sporns 2010). In a given network, E_{loc} is defined as

$$E_{loc} = \frac{1}{N} \sum_{i}^{N} E_{glob}(i), \quad (5)$$

where N represents the total number of nodes in the network, and $E_{glob}(i)$ represents the E_{glob} of the neighborhood nodes of node i. E_{loc} of the dynamic network was calculated as the average E_{loc} across all time windows.

We estimated both the E_{glob} and E_{loc} of the dynamic functional networks for every scan, and applied a mixed effect model to explore age effects on these two measures. To assess whether network efficiency was related to modular variability, we conducted a Pearson's correlation analysis between the mean modular variability of the brain and network efficiency across all scans, correcting for age, sex, and head motion effects. To further explore whether brain module dynamics mediated the age effects on network efficiency, we performed a single-level mediation analysis, with age, mean modular variability of the brain, and network efficiency (i.e., E_{glob} and E_{loc}), set, respectively, as the independent variable (X), mediator (M), and dependent variable (Y). Finally, to differentiate the contribution of different functional systems to the mediation effect, we employed a parallel multiple mediation analysis, with the mean modular variability of each of the six source systems (i.e., the somatomotor, default-mode, frontoparietal, dorsal attention, ventral attention, and visual systems) designated as mediators. In each mediation model, the explained fraction of the total effect for a given indirect path was defined as the product of the standard regression coefficients along this path divided by the sum of the products for all paths. The mediation analysis was performed using the PROCESS plugin in SPSS (Preacher and Hayes 2008). We then performed bootstrapping (n = 5000) to assess the statistical significance of the mediation analysis, for which a 95% confidence interval without 0 was equivalent to a significance level of 0.05 (Preacher and Hayes 2004).

Relationship Between Developmental Changes in Brain Network Dynamics and Gene Expression Profiles

To investigate the association between developmental changes in brain network dynamics and gene expression profiles, we used brain-wide gene expression data publicly available from the Allen Human Brain Atlas (http://human.brain-map.org/) (Hawrylycz et al. 2012). This atlas contains 3702 tissue samples from six donors, and provides their accurate MNI coordinates. Samples from two donors cover the whole brain, and the samples from the remaining four donors cover only the left hemisphere. Using the minimally processed data provided in the Allen Human Brain Atlas (http://help.brainmap.org/display/humanbrain/Documentation), we carried out the following procedures. First, we removed samples located in the brain stem and cerebellum, and re-annotated the gene names of probes for the remaining 2748 samples. Secondly, we used the intensity-based filtering method (Arnatkevičiūtė et al. 2019) to filter the data. For each gene, its expression level in a given sample was obtained by averaging the expression values across all detecting probes. Next, we normalized the expression data using the scaled robust sigmoid (SRS) algorithm (Fulcher et al. 2013) (see Supplement for further details). We then matched the MNI coordinates of each sample to the random-1024 parcellation scheme of the adult group using the nearest-point search algorithm. Each sample was then assigned to one of the brain nodes. For each node, expression data for each gene were obtained by first averaging the data across samples from the same donor, and then averaging the nodal expression data across donors. Using this process, for each node covered with samples, we obtained gene expression data for 15 745 genes. The preprocessing of gene expression data described above was performed by referencing the code at https://github.com/BMHLab/AHBAprocessing (Arnatkevičiūtė et al. 2019). As gene expression data for the right hemisphere were available from only two donors, to improve the reliability, we used left hemisphere gene expression data from all six donors for the subsequent brain network-gene association analysis.

To examine whether the spatial inhomogeneity in developmental changes in nodal modular variability was associated with gene expression levels, we performed an across-node spatial similarity analysis in the left hemisphere. Of note, 415 nodes (81.2% in the left hemisphere) exhibited linear decreases with age (i.e., $\beta_{age} < 0$), wherein the gene expression data of 67 nodes were not available. Thus, we performed this association analysis across the remaining 348 brain nodes. For each of the 15 745 genes, we undertook a Pearson's correlation analyses to measure the spatial similarity between the gene expression profile and the magnitude of developmental changes (i.e., $|\beta_{age}|$) in modular variability. The significance level of the spatial similarity was determined by comparing the empirically observed value to a null distribution obtained by 10 000 permutations, during which surrogate maps of developmental changes were generated while preserving the spatial autocorrelation characteristics of the original map (Burt et al. 2020). Significantly correlated genes were

identified with an FDR-corrected $P < 0.05$ and further divided into two categories, i.e., genes showing a significant positive correlation with developmental changes in modular variability and those showing a significant negative correlation. Functional enrichment analyses were separately performed on these two categories of genes using the ToppGene Suite (https://toppgene.cchmc.org/) (Chen et al. 2009).

Statistical Modeling

Given the nature of the longitudinal rsfMRI data used in this study, we applied a mixed effect model to study the developmental trajectories of brain network measures (Laird and Ware 1982; Diggle and Kenward 1994). Such models are well suited for cases with missing data, irregular intervals between data measurements, or potential correlation between variables. To account for potential linear and quadratic age effects, we undertook separate analyses using two different models that, respectively, had a linear term and quadratic term as their highest order term. For each analysis, we used the maximum likelihood method to undertake parameter estimation, and applied the Akaike information criterion (AIC) (Akaike 1974) to select the optimal model with a lower AIC value. Specifically, the linear model was defined as

$$y_{ij} = \beta_0 + b_i + (\beta_{age} + b_{age,i})\,age_{ij} + \beta_{sex}sex_i + \beta_{mFD}mFD_{ij} + \varepsilon_{ij}. \quad (6)$$

The quadratic model was defined as

$$y_{ij} = \beta_0 + b_i + (\beta_{age1} + b_{age,i1})\,age_{ij} + (\beta_{age2} + b_{age,i2})\,age_{ij}^2 + \beta_{sex}sex_i + \beta_{mFD}mFD_{ij} + \varepsilon_{ij}. \quad (7)$$

In these models, y_{ij} represents the observed brain network measures of subject i at the jth scan, β_{age} represents the fixed age effect, $b_{age,i}$ represents the random effect of subject i, and ε_{ij} represents the residual of subject i at the jth scan. Sex and mean FD (mFD) were also included as covariates in the two models. Here, we used the statistical models to estimate age effects on the following measures: the modularity (Q_{mod}) of the dynamic networks, the mean and standard deviation of regional modular variability across the brain, nodal modular variability values, and network efficiency (E_{glob} and E_{loc}). All scatter plots illustrate fixed age effects after correction for random effects.

Validation Analyses

We further investigated whether our results were affected by head motion and network analysis strategies, specifically the choice of sliding window parameters (i.e., window length and step size), multilayer network model parameters (i.e., temporal coupling parameter ω and topological resolution parameter γ), and network thresholding strategies. First, previous studies suggest that head motion can introduce spatially inhomogeneous bias in the estimation of functional connectivity (Power et al. 2012; Power et al. 2015), which may affect the evaluation of developmental effects (Satterthwaite et al. 2013). To reduce the influence of head motion, we included Friston's 24 head motion parameters (Friston et al. 1996), the global brain signal, and "bad" time points (FD > 0.5 mm) as covariates during nuisance regression. The residual influence of head motion was assessed by calculating the Pearson's correlation coefficient between head motion (i.e., mean FD) and global network dynamics across scans. Then, we validated the main findings by including both "bad" time points (FD > 0.5 mm) and their adjacent volumes (one back and two forward) as motion-induced spike regressors during the nuisance regression (Power et al. 2013; Yan et al. 2013). Second, the selection of sliding window parameters affects the estimation of dynamic connectivity and thus the temporal characteristics of the functional networks (Hutchison et al. 2013; Shakil et al. 2016; Lurie et al. 2020). In our main analysis, we set the window length as 60 s, a timeframe which is able to reliably capture the temporal variations in the functional networks (Lurie et al. 2020). To assess the potential influence of the sliding window length on our findings, we reconstructed the dynamic networks using a window length of 100 s. In this validation analysis, we also investigated the potential influence of the step size. We set the step size as 3 TR (i.e., 6 s, namely one-tenth of the window size), which reduced the overlap between adjacent windows and ensured the adequate window number for subsequent statistical analysis. Third, in the multilayer network model, the temporal coupling parameter, ω, between adjacent windows has a strong impact on the reconfiguration of modular architecture between windows (Mucha et al. 2010). In addition to using $\omega = 1$ in our main analysis, we repeated the multilayer network analysis using $\omega = 0.5$ and 0.75, respectively. Additionally, we examined the influence of the topological resolution parameter γ, which affects the estimated module size, by setting γ as 0.9. Finally, we evaluated whether our findings were influenced by the network thresholding strategies applied in functional network construction, which can affect the estimation of the graph metrics (Bullmore and Bassett 2011). In our main analysis, the maturation of network topology was our principal focus, and we therefore generated binary networks with a fixed network density (i.e., 5%) to correct for intersubject differences in the number and strength of functional connectivities. To explore the influence of network density, we constructed binary networks with a density of 10%. In addition, we also constructed weighted functional networks with a density of 5% to assess the impact of connectivity strength.

Results

Spatial Patterns of Brain Network Dynamics in Children

We employed longitudinal rsfMRI data from a cohort of 305 typically developing children (age: 6–14 years). For comparison purposes, we also included cross-sectional rsfMRI data from a group of 61 healthy adults (age: 18–29 years). We found that individual brain networks in children exhibited a modular structure, with modularity (Q_{mod}) values ranging from 0.53 to 0.62 (mean ± std dev = 0.58 ± 0.02) and the number of modules (N_{mod}) ranging from 5.35 to 6.58 (mean ± std dev = 5.93 ± 0.21). To qualitatively illustrate the progressive developmental changes in the spatial pattern of brain dynamics between childhood and adolescence, we divided the 491 rsfMRI scans into eight age subgroups, with a 1-year interval between each subgroup. An average modular variability map was then generated for each age subgroup (Fig. 1C). We found that, at a group level, the spatial pattern of modular variability in the child brain network showed regional heterogeneity, with higher variability primarily observed in the frontal and parietal cortices, anterior/middle cingulate gyrus, and middle temporal gyrus, and the lowest modular variability observed in the visual cortex. This spatial pattern observed in the child

cohort was highly similar to that of the adult group (Pearson's correlations: range, 0.83–0.89; mean ± std dev = 0.88 ± 0.02, all $P_{corr} < 0.0001$). When mapping these regions against the eight functional systems (visual, somatomotor, dorsal attention, ventral attention, limbic, frontoparietal, default-mode, and subcortical), we also observed a corresponding similarity in the system-dependent distributions of modular variability between child and adult brains (Fig. 1D). Notably, the topography of modular variability at both the global and system levels develops in a progressive fashion from childhood through adolescence toward that found in the adult brain. Below, we report our quantitative analysis of the longitudinal development of brain network dynamics.

Developmental Changes in Brain Network Dynamics in Children

At the global level, the modularity, Q_{mod}, of the dynamic brain networks increased with age (linear model, $t = 4.77$, $P < 0.0001$, Fig. 2A, left), suggesting enhanced functional segregation of network modules with age. The global mean values of modular variability in the child brain decreased with age (linear model, $t = -3.28$, $P = 0.0011$, Fig. 2A, middle), while the standard deviation across regions increased with age (linear model, $t = 2.43$, $P = 0.015$, Fig. 2A, right). These results suggest that the temporal dynamics of brain networks tend to become more stabilized and more regionally differentiated as the brain develops from childhood to adolescence.

At the nodal level, we observed that brain regions that showed significant changes in modular variability with age (a total of 77 nodes) predominantly exhibited significant linear decreases in variability ($P < 0.05$, FDR corrected). These nodes (75 in total) following linear models were primarily distributed in the medial and lateral frontal and parietal cortices, supplementary motor area, and somatomotor cortex, and were primarily associated with the somatomotor (40%), default-mode (33.33%), and frontoparietal (17.33%) systems (Fig. 2B). The remaining nodes with significant linear decreases were spread across the dorsal attention, ventral attention, and visual systems. For ease of reference, these systems were referred to as the six "source systems". For each source system, we explored the cognitive functions associated with these regions based on the NeuroSynth meta-analytic database (Yarkoni et al. 2011). These regions were mainly associated with internal cognitive functions, social inference, and primary motor functions (Fig. 2C). Additionally, we identified one node in the left temporal-occipital junction showing a significant age-related linear increase, and another node in the left olfactory cortex showing a U-shaped quadratic age-related change ($P < 0.05$, FDR corrected). The AIC differences between the linear and the quadratic models were displayed at the regional level (Fig. S1).

Next, we examined how the age-related decreases in nodal modular variability were associated with the dynamic interplay between the different functional systems. Specifically, we assessed age effects on the modular co-occurrence between the six source systems (i.e., the somatomotor, default-mode, frontoparietal, dorsal attention, ventral attention, and visual systems) and all eight functional systems (referred to as the target systems) (Fig. 2D and 2E). We observed that, as age increased, nodes in the default-mode, frontoparietal and somatomotor systems showed significantly increased intrasystem co-occurrence, indicating enhanced functional specificity within these systems. In relation to intersystem co-occurrence, we found that significant increases in co-occurrence were primarily observed between transmodal areas (consisting of the default-mode/frontoparietal systems) and the subcortical system, as well as between the dorsal attention systems and the primary sensory systems (i.e., somatomotor and visual systems). Meanwhile, significant decreases in co-occurrence were mainly observed between the default-mode/frontoparietal systems and the primary sensory systems, as well as between the default-mode/frontoparietal system and the attention systems. These findings suggest that the six source systems tend to be divided into two clusters, one comprising the transmodal areas and the subcortical system, and the other comprising the primary sensory and attention systems. During development, functional integration between these two clusters of systems decreases with age.

Brain Network Dynamics Mediates Age Effects on Communication Efficiency

We further explored whether the development of network dynamics might contribute to age-related changes in the information communication capability of brain networks, including global efficiency (E_{glob}) and local efficiency (E_{loc}). We found that E_{glob} of the functional networks decreased significantly with age (linear model, $t = -3.34$, $P < 0.001$), while E_{loc} increased significantly with age (linear model, $t = 4.98$, $P < 0.0001$) (Fig. 3A), indicating decreased information integration and increased information segregation between childhood and adolescence. Next, we examined the relationship between brain module dynamics and network efficiency (i.e., E_{glob} or E_{loc}) across individuals, controlling for age. We found that global mean values of modular variability showed a positive correlation with E_{glob} ($r = 0.67$, $P < 0.0001$) and a negative correlation with E_{loc} ($r = -0.63$, $P < 0.0001$) (Fig. 3B). These findings indicate that the dynamic module switching of brain regions is associated with integrated and segregated processing in brain networks.

Given the age-related changes in both network efficiency and brain module dynamics, we assessed whether the relationship between age and network efficiency was mediated by brain module dynamics. We performed a mediation analysis and found that the global mean value of modular variability had a significant mediation effect on the relationship between age and E_{glob} and E_{loc} ($P < 0.05$ for both, bootstrapped $n = 5000$) (Fig. 3C). To further determine the specific brain systems contributing to the mediation effects, we performed a parallel multiple mediation analysis and found that modular variability of the default-mode, frontoparietal, somatomotor, and visual systems exhibited significant mediation effects on the relationship between age and E_{glob} and E_{loc} (all $Ps < 0.05$, bootstrapped $n = 5000$), while modular variability of the attention (i.e., dorsal and ventral attention) system did not (Tables S1 and S2). The explained fraction of the total effect in the mediation models varied across functional systems, being highest in the somatomotor system, followed by the default-mode, visual, and frontoparietal systems for both E_{glob} and E_{loc}. These findings suggest that the reduction in module dynamics (i.e., network switching) between childhood and adolescence, in particular the reduced dynamics in the somatomotor and default-mode systems, significantly mediates the development of brain network communication efficiency to its mature state in the adult brain.

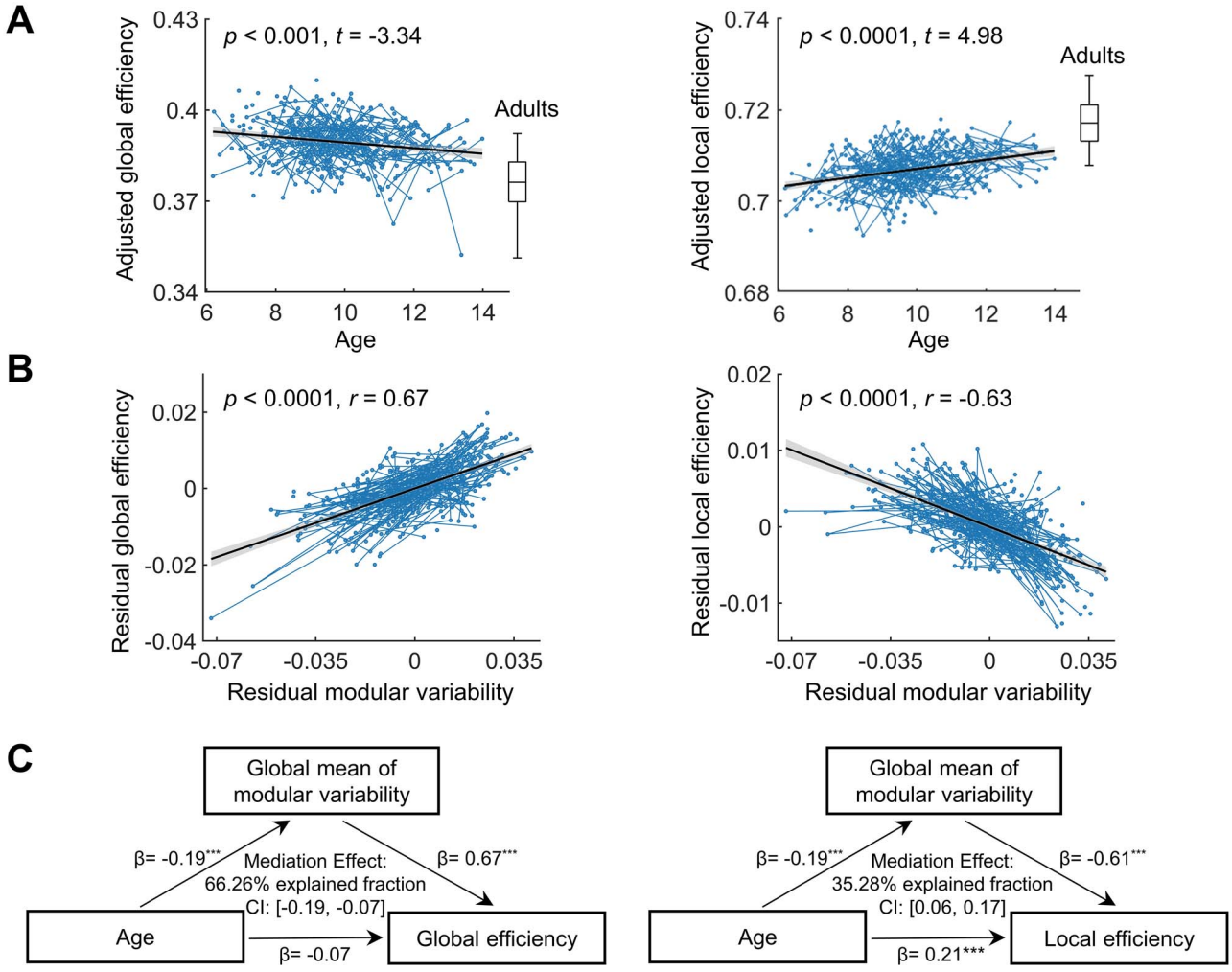

Figure 3. Relationship between age, brain dynamics, and network efficiency in children. **(A)** Age effects on global efficiency and local efficiency in the dynamic functional networks. Boxplots represent the distribution median, and the 25th and 75th percentiles of the adult group. **(B)** Relationship between modular variability and network efficiency in children. **(C)** Mediating effects of modular variability on developmental changes in global efficiency (left) and local efficiency (right) (all *P*s < 0.05, bootstrapped $n = 5000$). ***, $P < 0.001$. In **(A)** and **(B)**, the blue lines connecting scattered points represent longitudinal scans of the same child. The adjusted value in **(A)** denotes the measure of interest corrected for sex, head motion, and random age effects. The residual value in **(B)** denotes the measure of interest corrected for sex, head motion, and fixed and random age effects. We used a mixed effect model to estimate age effects.

Linking Developmental Network Dynamics in Children with Gene Transcriptional Profiles

We used univariate analysis to explore the spatial association between gene transcriptional profiles and the magnitude of regional developmental changes (i.e., $|\beta_{age}|$) (Fig. 4A and 4B). A total of 4551 genes were identified as showing a significant correlation with developmental changes in modular variability ($P < 0.05$, FDR corrected). Of these, 2190 genes showed a positive correlation and 2361 genes showed a negative correlation. The 10 genes showing the highest positive correlations are listed in Figure 4C (see Table S3 for all genes showing significant positive correlations). Gene ontology annotation analysis revealed that the positively correlated genes were associated with significant enrichment of biological processes, primarily those involving ion transport and nucleobase-containing compound transport ($P < 0.05$, FDR corrected) (Fig. 4D). For the enrichment of biological processes related to the negatively correlated genes, please see Table S4. We also considered a multivariate method of partial least squares (PLS) regression, which can incorporate the contribution from multiple genes (Whitaker et al. 2016; Li et al. 2021). The most significant GO term of ion transport obtained by the univariate approach was consistently observed by the PLS analysis (Fig. S2) (see Supplement for details).

Validations

To demonstrate the robustness of our main findings, we accessed the influence of several analysis strategies, including: i) testing for the residual head motion effects (post nuisance regression) and a more stringent spike regression strategy; ii) a longer sliding window length (100 s) and a wider step size (3 TR); iii) weaker temporal coupling parameters ($\omega = 0.5$ and 0.75) and a weaker topological resolution parameter ($\gamma = 0.9$); and iv) an increased network density (density = 10%) and a different network type (i.e., weighted as opposed to binary network).

We found that the head motion parameter of mean FD did not show a significant correlation with modular variability (Fig. S3), suggesting a weak influence of head motion on the observed developmental changes in brain network dynamics. We also found that, overall, the application of different analysis strategies did not affect or alter our main conclusions (Figs S4–S7).

Discussion

Using longitudinal rsfMRI data from a large cohort of healthy children, we demonstrate for the first time the development of brain network dynamics between childhood and adolescence and its connection with gene expression profiles. Specifically, modular dynamics in the brain network become progressively more stable as the brain matures, and is correlated with the transcriptional profiles of genes enriched for ion transport and nucleobase-containing compound transport. Changes in modular variability occur primarily in the default-mode, frontoparietal, and somatomotor systems. The development of more stable network dynamics mediates age-related changes of segregated and integrated processing in the brain, indicating an enhancement in the functional specialization of brain networks during this period. Together, these findings highlight the progressive stabilization of network switching between childhood and adolescence and describe the related gene expression profiles, providing insights into the understanding of typical and atypical development. Further, where the majority of previous developmental connectomics studies have mainly focused on dynamic functional connectivity patterns (Hutchison and Morton 2015; Qin et al. 2015; Ryali et al. 2016; Marusak et al. 2017; Faghiri et al. 2018; Medaglia et al. 2018), our study includes a specific investigation of the maturation of dynamic network topology during childhood and adolescence and the associated cognitive implications, greatly increasing the current knowledge on human brain development.

In the course of our investigation, we also observed that the topography of dynamic modular configurations during childhood and adolescence followed an adult-like spatial pattern. Evidence from adults indicates that during rest, brain regions spontaneously switch between functional modules in a spatially heterogeneous way, such that the association cortex shows higher temporal variability than the primary cortex (Chen et al. 2016; Liao et al. 2017; Pedersen et al. 2018; Liu et al. 2020). Highly variable regions usually act as flexible hubs to maintain efficient intermodule communication and promote cognitive flexibility (Schaefer et al. 2014; Yin et al. 2020). The spatial pattern observed from our child rsfMRI dataset showed a spatial distribution of modular variability similar to that of the adult brain described in previous studies. A similar spatial pattern was also observed in a previous study on functional module switching in infants (Yin et al. 2020). Combining our observations with prior findings regarding the adult brain (Chen et al. 2016; Liao et al. 2017; Pedersen et al. 2018; Liu et al. 2020) and the infant brain (Yin et al. 2020), we speculate that the spatially heterogeneous pattern is a common and underlying property that reflects the regional diversity in brain module dynamics.

The age-related decrease in functional modular variability may be related with the development of white matter structural connections. Temporal variability in functional connectivity strength has been demonstrated to be structurally constrained by white matter tracts (Deco et al. 2011; Liao et al. 2015; Zhang et al. 2016; Fukushima et al. 2018). More specifically, two brain regions linked by direct structural connections (i.e., white matter tracts) tend to show smaller temporal variability in functional connectivity strength than regions without direct structural connections, and the greater the strength of a direct structural connection, the smaller the temporal variability of the functional connectivity strength between the regions (Liao et al. 2015). Between childhood and adolescence, white matter tracts undergo profound refinements, including regressive processes (e.g., elimination of circuits, axonal projections, or synapses) and progressive myelination at the microscopic scale (Tau and Peterson 2010; Vértes and Bullmore 2015), and heterogeneous increases in structural connectivity strength at the macroscopic scale (Huang et al. 2015; Zhao et al. 2015). Given that structure–function coupling increases with age (van den Heuvel et al. 2015; Baum et al. 2020), the development of the white matter structural network may reduce regional switching frequency between functional modules and thereby promote the development of modular dynamics in the brain toward an adult level of stability.

Enhanced functional segregation during development has been identified in previous neurodevelopmental studies which applied a static functional connectivity approach (Stevens et al. 2009; Dosenbach et al. 2010; Gu et al. 2015; Cao et al. 2016). This is further confirmed by our findings that functional modularity in dynamic networks also increases with age. Consistent with the developmental changes in functional modularity, we also observed that, between childhood and adolescence, global network efficiency decreased and local network efficiency increased with age. Interestingly, we found that regional modular variability, especially that of the default-mode and somatomotor systems, significantly mediated the relationship between age and network efficiency. Prior studies in adults have demonstrated that dynamic adjustments in connectivity, especially connectivity adjustments in the default-mode network, induce fluctuations in network efficiency over time (Zalesky et al. 2014; de Pasquale et al. 2016). Thus, it is reasonable to postulate that, between childhood and adolescence, reduced modular variability in the default-mode system contributes to changes in intermodule information communication, affecting the development of communication efficiency in the dynamic functional networks.

In developmental cognitive neuroscience, the theory of interactive specialization (Johnson 2011) posits that during postnatal development, the function of brain regions becomes more specialized, as a result of the age-related reconfiguration of interregional interactions driven by intrinsic activities or environmental stimuli. Considering that brain module dynamics plays a crucial role in individual cognition (e.g., working memory) and behavior (e.g., motor skill learning) in adults (Bassett et al. 2011; Braun et al. 2015; Shine and Poldrack 2018), the reduction in regional module variability and the changes in network efficiency observed in our study may be related to individual refinements in these capabilities during childhood and adolescence. Consistent with this, we found that the regions showing most significant decreases in modular variability were those primarily involved in self-referential thinking, social cognition, and motor functions. In addition, a previous study has suggested that network flexibility in the human brain decreases when turning a motor skill task into an automatic process after a period of training (Bassett et al. 2015). We found that segregation between the somatomotor system and high-order systems increased between childhood and adolescence, suggesting that the decrease in modular variability in this system

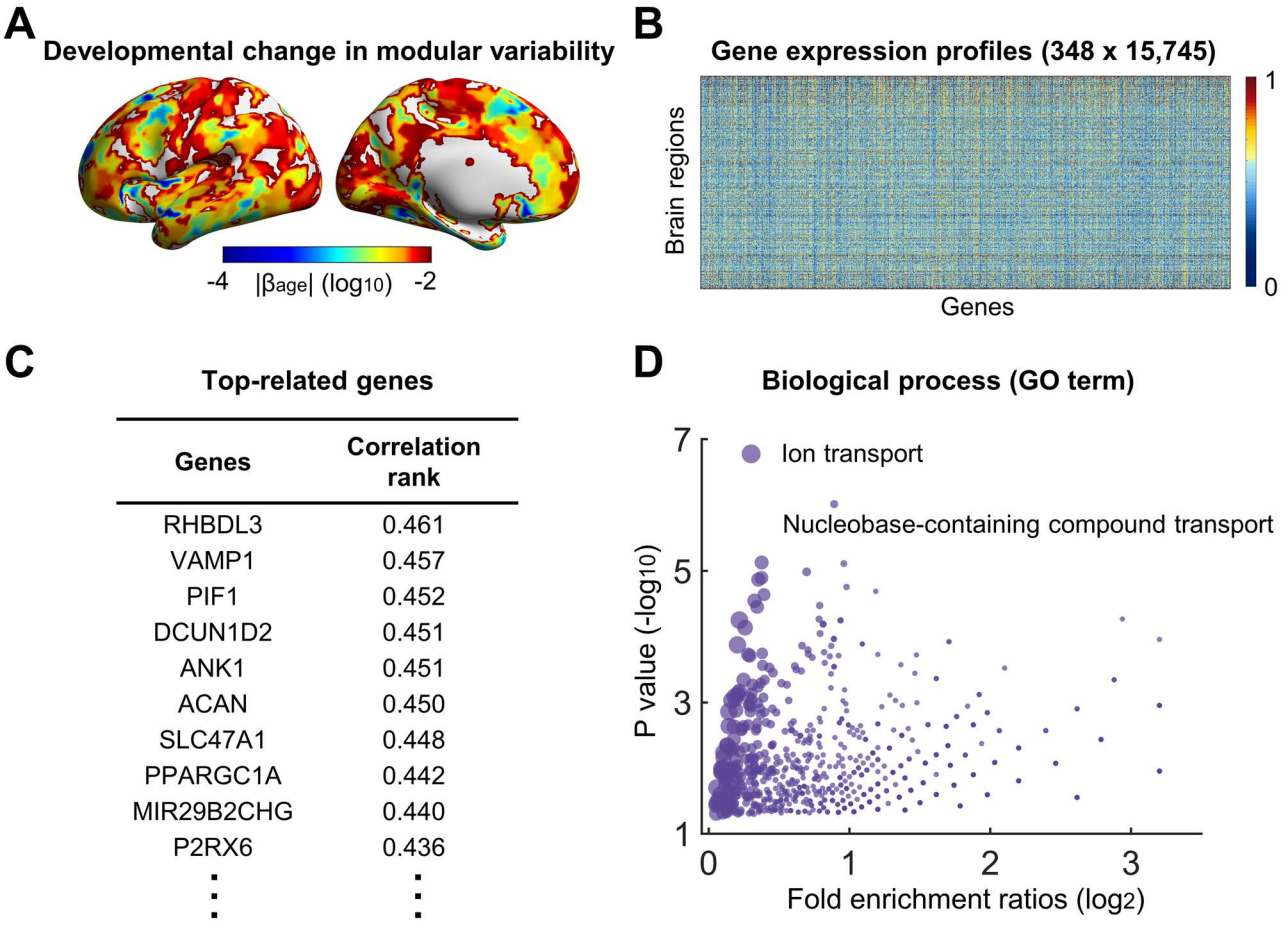

Figure 4. Association between developmental changes in brain network dynamics and gene expression profiles. **(A)** Spatial pattern of the magnitude of developmental changes (i.e., $|\beta_{age}|$) in modular variability for regions showing negative linear age effects in the left hemisphere. **(B)** Matrix of gene expression profiles. Each column represents the expression profile of each gene across the 348 nodes of interest. **(C)** Genes showing the highest positive correlations with the developmental change in regional modular variability. Only the top 10 genes are listed. Pearson's correlation coefficients were calculated within the set of nodes showing negative linear age effects. **(D)** Gene ontology (GO) terms of biological processes associated with genes showing significant positive correlations with the developmental change. The dots marked with text represent significant GO terms obtained with correction for multiple comparisons (FDR-corrected $P < 0.05$), and the remainder represents GO terms obtained without correction (uncorrected $P < 0.05$). The dot size represents the number of genes that overlap with the corresponding GO term.

could be related to the refinement of somatomotor capabilities during this period. However, in contrast to our observations, one recent study found that regional module switching (i.e., flexibility), especially that of the primary system, showed significant increases with age during the first 2 years of life (Yin et al. 2020). This discrepancy may be attributable to the different developmental phases considered (infants versus school-age children) or to the application of different network construction strategies (i.e., absolute correlation thresholding versus fixed-density thresholding) in the two studies.

By performing a connectome-transcriptome association analysis, a recent study that we also undertook demonstrated that the spatial heterogeneity of module dynamics in the adult brain is shaped by the expression profile of the genes primarily associated with potassium ion transport (Liu et al. 2020). Nevertheless, the genetic basis underpinning the development of functional network dynamics remains poorly understood. Our work addresses this gap in knowledge by revealing that the maturation of brain module dynamics toward an adult-like state is associated with the expression profiles of genes associated with the enrichment of ion transport and nucleobase-containing compound transport. Ion transport is one of the most important functions of a neuron, facilitating the balance of ion concentrations in and out of the cell membrane and promoting the stability of brain neural circuits (Gibson et al. 2007). A recent computational modeling study further suggests that ion concentration dynamics causes spontaneous neuronal fluctuations (Krishnan et al. 2018), which may contribute to fluctuations in blood oxygenation level-dependent (BOLD)-fMRI signals (Schölvinck et al. 2010). In addition, nucleoside transport has been found to be dependent on ion concentrations (especially that of Na^+), and Na+/nucleoside cotransports are also an electrogenic process (Griffith and Jarvis 1996). Given the above, it makes sense that the development of adult-like modular dynamics is related to the transport of ions and nucleobase-containing compounds, which can affect interregional interactions by modulating neural activities.

Of the genes that were found in our study to be highly correlated with developmental changes in modular variability, several have also been identified in prior studies as being related to brain development. Specifically, ACAN (aggrecan) has been

found to control the maturation of glial cells during brain development (Dornowicz et al. 2008); the basic helix–loop–helix gene HES6 promotes neuronal differentiation (Bae et al. 2000); FGF9 (fibroblast growth factor 9) is crucial for the postnatal migration of cerebellar granule neurons (Lin et al. 2009); and Sema7A (semaphorins) regulates climbing fiber synapse elimination in the developing mouse brain (Uesaka et al. 2014). The identification of correlated genes provides novel clues for bridging the gap between our understanding of the developmental changes in brain network dynamics and our limited knowledge of the underlying biological mechanisms.

Several issues and future research topics deserve further consideration. First, we used postmortem gene expression data from adult donors obtained from the Allen Human Brain Atlas to explore the relationship between gene expression and the developmental changes of network dynamics in children. While the absolute expression levels of genes may change with age due to developmental effects, their spatial patterns do not seem to change greatly after birth (Kang et al. 2011). As our interest lies in the spatial pattern (i.e., relative values across regions) of gene expression profiles rather than exact expression values, the choice of gene expression data should not have a great influence on our findings. Nevertheless, the availability of cerebral cortex gene expression data for children and adolescents could be beneficial for future exploration of the molecular mechanisms underlying developmental network dynamics. Secondly, previous studies in adults have suggested that brain network dynamics show a relationship with cognitive flexibility (Chen et al. 2016; Liao et al. 2017; Yin et al. 2020) and individual task performance (Pedersen et al. 2018). How then is the progressive maturation of brain network dynamics during childhood and adolescence associated with the development of individual cognition and behavior? In this study, we measured the *n*-back working memory performance in children. Working memory is a central component of the executive function, which exhibits pronounced improvements during childhood and adolescence (Gur et al. 2012). Here, our preliminary results showed that the progressive stabilization of the module dynamics was significantly associated with an age-related enhancement in 2-back working memory performance (i.e., d-prime), especially that in the default-mode and sensorimotor systems (Fig. S8). In the future, more efforts should be devoted to exploring the cognitive implications of network dynamics during development. Finally, as abnormalities in the dynamic characteristics of functional brain networks have been observed in several neurodevelopmental disorders (e.g., attention-deficit/hyperactivity disorder (Ding et al. 2020) and autism spectrum disorder (Harlalka et al. 2019), delineating the typical developmental trajectory of brain network dynamics may provide novel clues for the early detection or diagnosis of atypical neurodevelopment.

Author Contributions

T.L., X.L., S.T., Q.D., and Y.H. designed the research; W.M., Y.W., M.H., G.Z., B.D., S.P., M.C., S.T., J.G., S.Q., S.T., and Q.D. collected the data; T.L. and X.L. performed the research; X.C., T.Z., Y.X., M.X., Y.X., X.S., Y.W., and Q.W. provided technical assistance; and T.L., X.L., T.Z., J.Z., and Y.H. wrote the paper.

Funding

The study was supported by the grant from National Key R&D Program of China (2018YFA0701402), the National Natural Science Foundation of China (Nos. 82021004, 81971690, 31830034, 81620108016, 11835003, 31221003, 31521063, and 81801783), the Changjiang Scholar Professorship Award (T2015027), the Beijing Brain Initiative of the Beijing Municipal Science & Technology Commission (Z181100001518003), and the Fundamental Research Funds for Central Universities (2019NTST24).

Notes

We thank the National Center for Protein Sciences at Peking University in Beijing, China, for assistance with MRI data acquisition. *Conflict of Interest*: None declared.

Data and Code Availability

Nodal time series of preprocessed rsfMRI signals and some other data supporting the results of this study are available at https://github.com/helab207/Development-of-brain-module-dynamics.

Codes used for the neuroimaging analysis and the statistical models are available at https://github.com/helab207/Development-of-brain-module-dynamics.

References

Akaike H. 1974. A new look at the statistical model identification. *IEEE Trans Automat Contr*. 19:716–723.

Arnatkevičiūtė A, Fulcher BD, Fornito A. 2019. A practical guide to linking brain-wide gene expression and neuroimaging data. *Neuroimage*. 189:353–367.

Ashburner J, Friston KJ. 2005. Unified segmentation. *Neuroimage*. 26:839–851.

Bae S, Bessho Y, Hojo M, Kageyama R. 2000. The bHLH gene Hes6, an inhibitor of Hes1, promotes neuronal differentiation. *Development*. 127:2933–2943.

Bassett DS, Wymbs NF, Porter MA, Mucha PJ, Carlson JM, Grafton ST. 2011. Dynamic reconfiguration of human brain networks during learning. *Proc Natl Acad Sci USA*. 108:7641–7646.

Bassett DS, Yang M, Wymbs NF, Grafton ST. 2015. Learning-induced autonomy of sensorimotor systems. *Nat Neurosci*. 18:744–751.

Baum GL, Cui ZX, Roalf DR, Ciric R, Betzel RF, Larsen B, Cieslak M, Cook PA, Xia CH, Moore TM, et al. 2020. Development of structure-function coupling in human brain networks during youth. *Proc Natl Acad Sci USA*. 117:771–778.

Berk LE. 2017. *Development through the lifespan*. 7th ed. London: Pearson.

Bertolero MA, Yeo BTT, D'Esposito M. 2015. The modular and integrative functional architecture of the human brain. *Proc Natl Acad Sci USA*. 112:E6798–E6807.

Blondel VD, Guillaume JL, Lambiotte R, Lefebvre E. 2008. Fast unfolding of communities in large networks. *J Stat Mech*. 2008:P10008.

Braun U, Schafer A, Walter H, Erk S, Romanczuk-Seiferth N, Haddad L, Schweiger JI, Grimm O, Heinz A, Tost H, et al. 2015. Dynamic reconfiguration of frontal brain networks during executive cognition in humans. *Proc Natl Acad Sci USA*. 112:11678–11683.

Bullmore E, Sporns O. 2012. The economy of brain network organization. *Nat Rev Neurosci*. 13:336–349.

Bullmore ET, Bassett DS. 2011. Brain graphs: graphical models of the human brain connectome. *Annu Rev Clin Psychol*. 7:113–140.

Burt JB, Helmer M, Shinn M, Anticevic A, Murray JD. 2020. Generative modeling of brain maps with spatial autocorrelation. *Neuroimage*. 220:117038.

Cao M, Huang H, Peng Y, Dong Q, He Y. 2016. Toward developmental connectomics of the human brain. *Front Neuroanat*. 10:25.

Chen J, Bardes EE, Aronow BJ, Jegga AG. 2009. ToppGene Suite for gene list enrichment analysis and candidate gene prioritization. *Nucleic Acids Res*. 37:W305–W311.

Chen T, Cai W, Ryali S, Supekar K, Menon V. 2016. Distinct global brain dynamics and spatiotemporal organization of the salience network. *PLoS Biol*. 14:e1002469.

Chung WS, Clarke LE, Wang GX, Stafford BK, Sher A, Chakraborty C, Joung J, Foo LC, Thompson A, Chen CF, et al. 2013. Astrocytes mediate synapse elimination through MEGF10 and MERTK pathways. *Nature*. 504:394–400.

de Pasquale F, Della Penna S, Sporns O, Romani GL, Corbetta M. 2016. A dynamic core network and global efficiency in the resting human brain. *Cereb Cortex*. 26:4015–4033.

Deco G, Jirsa VK, McIntosh AR. 2011. Emerging concepts for the dynamical organization of resting-state activity in the brain. *Nat Rev Neurosci*. 12:43–56.

Diggle P, Kenward MG. 1994. Informative drop-out in longitudinal data-analysis. *J R Stat Soc Ser C Appl Stat*. 43:49–93.

Ding CL, Xiang J, Cui XH, Wang XY, Li DD, Cheng C, Wang B. 2020. Abnormal dynamic community structure of patients with attention-deficit/hyperactivity disorder in the resting state. *J Atten Disord*. doi: 10.1177/1087054720959712.

Dornowicz MS, Sanders TA, Ragsdale CW, Schwartz NB. 2008. Aggrecan is expressed by embryonic brain glia and regulates astrocyte development. *Dev Biol*. 315:114–124.

Dosenbach NUF, Nardos B, Cohen AL, Fair DA, Power JD, Church JA, Nelson SM, Wig GS, Vogel AC, Lessov-Schlaggar CN, et al. 2010. Prediction of individual brain maturity using fMRI. *Science*. 329:1358–1361.

Douet V, Chang LD, Cloak C, Ernst T. 2014. Genetic influences on brain developmental trajectories on neuroimaging studies: from infancy to young adulthood. *Brain Imaging Behav*. 8:234–250.

Emery B, Agalliu D, Cahoy JD, Watkins TA, Dugas JC, Mulinyawe SB, Ibrahim A, Ligon KL, Rowitch DH, Barres BA. 2009. Myelin gene regulatory factor is a critical transcriptional regulator required for CNS myelination. *Cell*. 138:172–185.

Faghiri A, Stephen JM, Wang YP, Wilson TW, Calhoun VD. 2018. Changing brain connectivity dynamics: from early childhood to adulthood. *Hum Brain Mapp*. 39:1108–1117.

Fair DA, Cohen AL, Dosenbach NUF, Church JA, Miezin FM, Barch DM, Raichle ME, Petersen SE, Schlaggar BL. 2008. The maturing architecture of the brain's default network. *Proc Natl Acad Sci USA*. 105:4028–4032.

Fair DA, Cohen AL, Power JD, Dosenbach NUF, Church JA, Miezin FM, Schlaggar BL, Petersen SE. 2009. Functional brain networks develop from a "local to distributed" organization. *PLoS Comput Biol*. 5:e1000381.

Fair DA, Dosenbach NUF, Church JA, Cohen AL, Brahmbhatt S, Miezin FM, Barch DM, Raichle ME, Petersen SE, Schlaggar BL. 2007. Development of distinct control networks through segregation and integration. *Proc Natl Acad Sci USA*. 104: 13507–13512.

Fan F, Liao X, Lei T, Zhao T, Xia M, Men W, Wang Y, Hu M, Liu J, Qin S, et al. 2021. Development of the default-mode network during childhood and adolescence: a longitudinal resting-state fMRI study. *Neuroimage*. 226:117581.

Finc K, Bonna K, He XS, Lydon-Staley DM, Kuhn S, Duch W, Bassett DS. 2020. Dynamic reconfiguration of functional brain networks during working memory training. *Nat Commun*. 11:1–15.

Fornito A, Arnatkevičiūtė A, Fulcher B. 2019. Bridging the gap between connectome and transcriptome. *Trends Cogn Sci*. 23:34–50.

Fox MD, Zhang DY, Snyder AZ, Raichle ME. 2009. The global signal and observed anticorrelated resting state brain networks. *J Neurophysiol*. 101:3270–3283.

Friston KJ, Williams S, Howard R, Frackowiak RSJ, Turner R. 1996. Movement-related effects in fMRI time-series. *Magn Reson Med*. 35:346–355.

Fukushima M, Betzel RF, He Y, van den Heuvel MP, Zuo X, Sporns O. 2018. Structure-function relationships during segregated and integrated network states of human brain functional connectivity. *Brain Struct Funct*. 223:1091–1106.

Fulcher BD, Little MA, Jones NS. 2013. Highly comparative time-series analysis: the empirical structure of time series and their methods. *J R Soc Interface*. 10:20130048.

Gibson GE, Dienel GA, Purdon A, Rapoport SE. 2007. *Handbook of neurochemistry and molecular neurobiology*. New York, NY: Springer.

Grayson DS, Fair DA. 2017. Development of large-scale functional networks from birth to adulthood: a guide to the neuroimaging literature. *Neuroimage*. 160:15–31.

Griffith DA, Jarvis SM. 1996. Nucleoside and nucleobase transport systems of mammalian cells. *Biochim Biophys Acta Biomembr*. 1286:153–181.

Gu S, Satterthwaite TD, Medaglia JD, Yang M, Gur RE, Gur RC, Bassett DS. 2015. Emergence of system roles in normative neurodevelopment. *Proc Natl Acad Sci USA*. 112:13681–13686.

Gur RC, Richard J, Calkins ME, Chiavacci R, Hansen JA, Bilker WB, Loughead J, Connolly JJ, Qiu H, Mentch FD. 2012. Age group and sex differences in performance on a computerized neurocognitive battery in children age 8–21. *Neuropsychology*. 26:251.

Harlalka V, Bapi RS, Vinod PK, Roy D. 2019. Atypical flexibility in dynamic functional connectivity quantifies the severity in autism spectrum disorder. *Front Hum Neurosci*. 13:6.

Hawrylycz MJ, Lein ES, Guillozet-Bongaarts AL, Shen EH, Ng L, Miller JA, van de Lagemaat LN, Smith KA, Ebbert A, Riley ZL, et al. 2012. An anatomically comprehensive atlas of the adult human brain transcriptome. *Nature*. 489:391–399.

He Y, Wang J, Wang L, Chen Z, Yan C, Yang H, Tang H, Zhu C, Gong Q, Zang Y, Evans AC. 2009. Uncovering intrinsic modular organization of spontaneous brain activity in humans. *PLoS One*. 4:e5226.

Huang H, Shu N, Mishra V, Jeon T, Chalak L, Wang ZJ, Rollins N, Gong G, Cheng H, Peng Y, et al. 2015. Development of human brain structural networks through infancy and childhood. *Cereb Cortex*. 25:1389–1404.

Hutchison RM, Morton JB. 2015. Tracking the brain's functional coupling dynamics over development. *J Neurosci*. 35:6849–6859.

Hutchison RM, Morton JB. 2016. It's a matter of time: reframing the development of cognitive control as a modification of the brain's temporal dynamics. *Dev Cogn Neurosci*. 18:70–77.

Hutchison RM, Womelsdorf T, Allen EA, Bandettini PA, Calhoun VD, Corbetta M, Penna S, Duyn JH, Glover GH, Gonzalez-Castillo J, et al. 2013. Dynamic functional connectivity: promise, issues, and interpretations. *Neuroimage*. 80: 360–378.

Johnson MB, Kawasawa YI, Mason CE, Krsnik Ž, Coppola G, Bogdanović D, Geschwind DH, Mane SM, State MW, Šestan N. 2009. Functional and evolutionary insights into human brain development through global transcriptome analysis. *Neuron*. 62:494–509.

Johnson MH. 2011. Interactive specialization: a domain-general framework for human functional brain development? *Dev Cogn Neurosci*. 1:7–21.

Kang HJ, Kawasawa YI, Cheng F, Zhu Y, Xu X, Li M, Sousa AMM, Pletikos M, Meyer KA, Sedmak G, et al. 2011. Spatio-temporal transcriptome of the human brain. *Nature*. 478:483–489.

Krishnan GP, González OC, Bazhenov M. 2018. Origin of slow spontaneous resting-state neuronal fluctuations in brain networks. *Proc Natl Acad Sci USA*. 115:6858–6863.

Laird NM, Ware JH. 1982. Random-effects models for longitudinal data. *Biometrics*. 38:963–974.

Latora V, Marchiori M. 2001. Efficient behavior of small-world networks. *Phys Rev Lett*. 87:198701.

Li J, Seidlitz J, Suckling J, Fan F, Ji G, Meng Y, Yang S, Wang K, Qiu J, Chen H. 2021. Cortical structural differences in major depressive disorder correlate with cell type-specific transcriptional signatures. *Nat Commun*. 12:1–14.

Liao X, Cao M, Xia M, He Y. 2017. Individual differences and time-varying features of modular brain architecture. *Neuroimage*. 152:94–107.

Liao X, Yuan L, Zhao T, Dai Z, Shu N, Xia M, Yang Y, Evans A, He Y. 2015. Spontaneous functional network dynamics and associated structural substrates in the human brain. *Front Hum Neurosci*. 9:478.

Lin Y, Chen L, Lin C, Luo Y, Tsai RYL, Wang F. 2009. Neuron-derived FGF9 is essential for scaffold formation of Bergmann radial fibers and migration of granule neurons in the cerebellum. *Dev Biol*. 329:44–54.

Liu J, Xia M, Wang X, Liao X, He Y. 2020. The spatial organization of the chronnectome associates with cortical hierarchy and transcriptional profiles in the human brain. *Neuroimage*. 222:117296.

Lurie DJ, Kessler D, Bassett DS, Betzel RF, Breakspear M, Kheilholz S, Kucyi A, Liegeois R, Lindquist MA, McIntosh AR, et al. 2020. Questions and controversies in the study of time-varying functional connectivity in resting fMRI. *Netw Neurosci*. 4:30–69.

Marusak HA, Calhoun VD, Brown S, Crespo LM, Sala-Hamrick K, Gotlib IH, Thomason ME. 2017. Dynamic functional connectivity of neurocognitive networks in children. *Hum Brain Mapp*. 38:97–108.

Medaglia JD, Satterthwaite TD, Kelkar A, Ciric R, Moore TM, Ruparel K, Gur RC, Gur RE, Bassett DS. 2018. Brain state expression and transitions are related to complex executive cognition in normative neurodevelopment. *Neuroimage*. 166:293–306.

Meunier D, Lambiotte R, Bullmore ET. 2010. Modular and hierarchically modular organization of brain networks. *Front Neurosci*. 4:200.

Mucha PJ, Richardson T, Macon K, Porter MA, Onnela JP. 2010. Community structure in time-dependent, multiscale, and multiplex networks. *Science*. 328:876–878.

Murphy K, Fox MD. 2017. Towards a consensus regarding global signal regression for resting state functional connectivity MRI. *Neuroimage*. 154:169–173.

Pedersen M, Zalesky A, Omidvarnia A, Jackson GD. 2018. Multilayer network switching rate predicts brain performance. *Proc Natl Acad Sci USA*. 115:13376–13381.

Power JD, Barnes KA, Snyder AZ, Schlaggar BL, Petersen SE. 2012. Spurious but systematic correlations in functional connectivity MRI networks arise from subject motion. *Neuroimage*. 59:2142–2154.

Power JD, Barnes KA, Snyder AZ, Schlaggar BL, Petersen SE. 2013. Steps toward optimizing motion artifact removal in functional connectivity MRI; a reply to Carp. *Neuroimage*. 76:439–441.

Power JD, Schlaggar BL, Petersen SE. 2015. Recent progress and outstanding issues in motion correction in resting state fMRI. *Neuroimage*. 105:536–551.

Preacher KJ, Hayes AF. 2004. SPSS and SAS procedures for estimating indirect effects in simple mediation models. *Behav Res Methods Instrum Comput*. 36:717–731.

Preacher KJ, Hayes AF. 2008. Asymptotic and resampling strategies for assessing and comparing indirect effects in multiple mediator models. *Behav Res Methods*. 40:879–891.

Qin J, Chen S, Hu D, Zeng L, Fan Y, Chen X, Shen H. 2015. Predicting individual brain maturity using dynamic functional connectivity. *Front Hum Neurosci*. 9:418.

Richiardi J, Altmann A, Milazzo AC, Chang C, Chakravarty MM, Banaschewski T, Barker GJ, Bokde ALW, Bromberg U, Buchel C, et al. 2015. Correlated gene expression supports synchronous activity in brain networks. *Science*. 348:1241–1244.

Rubinov M, Sporns O. 2010. Complex network measures of brain connectivity: uses and interpretations. *Neuroimage*. 52:1059–1069.

Ryali S, Supekar K, Chen T, Kochalka J, Cai W, Nicholas J, Padmanabhan A, Menon V. 2016. Temporal dynamics and developmental maturation of salience, default and central-executive network interactions revealed by variational bayes hidden markov modeling. *PLoS Comput Biol*. 12:e1005138.

Sato JR, Salum GA, Gadelha A, Picon FA, Pan PM, Vieira G, Zugman A, Hoexter MQ, Anes M, Moura LM, et al. 2014. Age effects on the default mode and control networks in typically developing children. *J Psychiatr Res*. 58:89–95.

Satterthwaite TD, Wolf DH, Ruparel K, Erus G, Elliott MA, Eickhoff SB, Gennatas ED, Jackson C, Prabhakaran K, Smith A, et al. 2013. Heterogeneous impact of motion on fundamental patterns of developmental changes in functional connectivity during youth. *Neuroimage*. 83:45–57.

Schaefer A, Margulies DS, Lohmann G, Gorgolewski KJ, Smallwood J, Kiebel SJ, Villringer A. 2014. Dynamic network participation of functional connectivity hubs assessed by resting-state fMRI. *Front Hum Neurosci*. 8:195.

Schölvinck ML, Maier A, Ye FQ, Duyn JH, Leopold DA. 2010. Neural basis of global resting-state fMRI activity. *Proc Natl Acad Sci USA*. 107:10238–10243.

Shakil S, Lee CH, Keilholz SD. 2016. Evaluation of sliding window correlation performance for characterizing dynamic functional connectivity and brain states. *Neuroimage*. 133: 111–128.

Shine JM, Poldrack RA. 2018. Principles of dynamic network reconfiguration across diverse brain states. *Neuroimage*. 180:396–405.

Sporns O, Betzel RF. 2016. Modular brain networks. *Annu Rev Psychol*. 67:613–640.

Steen M, Hayasaka S, Joyce K, Laurienti P. 2011. Assessing the consistency of community structure in complex networks. *Phys Rev E*. 84:016111.

Stevens MC, Pearlson GD, Calhoun VD. 2009. Changes in the interaction of resting-state neural networks from adolescence to adulthood. *Hum Brain Mapp*. 30:2356–2366.

Supekar K, Musen M, Menon V. 2009. Development of large-scale functional brain networks in children. *PLoS Biol*. 7:e1000157.

Tau GZ, Peterson BS. 2010. Normal development of brain circuits. *Neuropsychopharmacology*. 35:147–168.

Tzourio-Mazoyer N, Landeau B, Papathanassiou D, Crivello F, Etard O, Delcroix N, Mazoyer B, Joliot M. 2002. Automated anatomical labeling of activations in SPM using a macroscopic anatomical parcellation of the MNI MRI single-subject brain. *Neuroimage*. 15:273–289.

Uesaka N, Uchigashima M, Mikuni T, Nakazawa T, Nakao H, Hirai H, Aiba A, Watanabe M, Kano M. 2014. Retrograde semaphorin signaling regulates synapse elimination in the developing mouse brain. *Science*. 344:1020–1023.

van den Heuvel MP, Kersbergen KJ, de Reus MA, Keunen K, Kahn RS, Groenendaal F, de Vries LS, Benders MJ. 2015. The neonatal connectome during preterm brain development. *Cereb Cortex*. 25:3000–3013.

Vértes PE, Bullmore ET. 2015. Annual research review: growth connectomics - the organization and reorganization of brain networks during normal and abnormal development. *J Child Psychol Psychiatry*. 56:299–320.

Vértes PE, Rittman T, Whitaker KJ, Romero-Garcia R, Váša F, Kitzbichler MG, Wagstyl K, Fonagy P, Dolan RJ, Jones PB, et al. 2016. Gene transcription profiles associated with inter-modular hubs and connection distance in human functional magnetic resonance imaging networks. *Philos Trans R Soc Lond B Biol Sci*. 371:20150362.

Vinh NX, Epps J, Bailey J. 2010. Information theoretic measures for clusterings comparison: variants, properties, normalization and correction for chance. *J Mach Learn Res*. 11:2837–2854.

Whitaker KJ, Vértes PE, Romero-Garcia R, Váša F, Moutoussis M, Prabhu G, Weiskopf N, Callaghan MF, Wagstyl K, Rittman T. 2016. Adolescence is associated with genomically patterned consolidation of the hubs of the human brain connectome. *Proc Natl Acad Sci USA*. 113:9105–9110.

Xia M, Wang J, He Y. 2013. BrainNet Viewer: a network visualization tool for human brain connectomics. *PLoS One*. 8:e68910.

Yan C, Cheung B, Kelly C, Colcombe S, Craddock RC, Di Martino A, Li Q, Zuo X, Castellanos FX, Milham MP. 2013. A comprehensive assessment of regional variation in the impact of head micromovements on functional connectomics. *Neuroimage*. 76:183–201.

Yan C, Wang X, Zuo X, Zang Y. 2016. DPABI: data processing & analysis for (resting-state) brain imaging. *Neuroinformatics*. 14:339–351.

Yarkoni T, Poldrack RA, Nichols TE, Van Essen DC, Wager TD. 2011. Large-scale automated synthesis of human functional neuroimaging data. *Nat Methods*. 8:665–670.

Yeo BTT, Krienen FM, Sepulcre J, Sabuncu MR, Lashkari D, Hollinshead M, Roffman JL, Smoller JW, Zoller L, Polimeni JR, et al. 2011. The organization of the human cerebral cortex estimated by intrinsic functional connectivity. *J Neurophysiol*. 106:1125–1165.

Yin W, Li T, Hung S, Zhang H, Wang L, Shen D, Zhu H, Mucha PJ, Cohen JR, Lin W. 2020. The emergence of a functionally flexible brain during early infancy. *Proc Natl Acad Sci USA*. 117:23904–23913.

Zalesky A, Fornito A, Cocchi L, Gollo LL, Breakspear M. 2014. Time-resolved resting-state brain networks. *Proc Natl Acad Sci USA*. 111:10341–10346.

Zalesky A, Fornito A, Harding IH, Cocchi L, Yucel M, Pantelis C, Bullmore ET. 2010. Whole-brain anatomical networks: does the choice of nodes matter? *Neuroimage*. 50:970–983.

Zhang J, Cheng W, Liu Z, Zhang K, Lei X, Yao Y, Becker B, Liu Y, Kendrick KM, Lu G, et al. 2016. Neural, electrophysiological and anatomical basis of brain-network variability and its characteristic changes in mental disorders. *Brain*. 139:2307–2321.

Zhao T, Cao M, Niu H, Zuo X, Evans A, He Y, Dong Q, Shu N. 2015. Age-related changes in the topological organization of the white matter structural connectome across the human lifespan. *Hum Brain Mapp*. 36:3777–3792.

Zhao T, Liao X, Fonov VS, Wang Q, Men W, Wang Y, Qin S, Tan S, Gao J, Evans A, et al. 2019. Unbiased age-specific structural brain atlases for Chinese pediatric population. *Neuroimage*. 189:55–70.

Zhong S, Zhang S, Fan X, Wu Q, Yan L, Dong J, Zhang H, Li L, Sun L, Pan N, et al. 2018. A single-cell RNA-seq survey of the developmental landscape of the human prefrontal cortex. *Nature*. 555:524–528.